

RESEARCH LETTER

10.1029/2018GL077060

Key Points:

- We obtain a new catalog of small events and repeating earthquakes in an ~4-year period before the 2015 Mw 8.4 Illapel earthquake
- The last episode of aseismic-slip transients are most significant at both sides of the Illapel rupture zone, suggesting a large-scale slow unlocking process
- Both seismicity and aseismic slip progressively accelerate around the epicenter, indicating the interplay of seismic and aseismic slip

Supporting Information:

- Supporting Information S1

Correspondence to:

L. Meng,
meng@ess.ucla.edu

Citation:

Huang, H., & Meng, L. (2018). Slow unlocking processes preceding the 2015 Mw 8.4 Illapel, Chile, earthquake. *Geophysical Research Letters*, 45. <https://doi.org/10.1029/2018GL077060>

Received 16 JAN 2018

Accepted 14 APR 2018

Accepted article online 23 APR 2018

Slow Unlocking Processes Preceding the 2015 Mw 8.4 Illapel, Chile, Earthquake

Hui Huang¹ and Lingsen Meng¹ 

¹Earth, Planetary, and Space Sciences, University of California, Los Angeles, CA, USA

Abstract On 16 September 2015, the Mw 8.4 Illapel earthquake occurred in central Chile with no intense foreshock sequences documented in the regional earthquake catalog. Here we employ the matched-filter technique based on an enhanced template data set of previously catalogued events. We perform a continuous search over an ~4-year period before the Illapel mainshock to recover the uncatalogued small events and repeating earthquakes. Repeating earthquakes are found both to the north and south of the mainshock rupture zone. To the south of the rupture zone, the seismicity and repeater-inferred aseismic slip progressively accelerate around the Illapel epicenter starting from ~140 days before the mainshock. This may indicate an unlocking process involving the interplay of seismic and aseismic slip. The acceleration culminates in a M 5.3 event of low-angle thrust mechanism, which occurred ~36 days before the Mw 8.4 mainshock. It is then followed by a relative quiescence in seismicity until the mainshock occurred. This quiescence might correspond to an intermediate period of stable slip before rupture initiation. In addition, to the north of the mainshock rupture area, the last aseismic-slip episode occurs within ~175–95 days before the mainshock and accumulates the largest amount of slip in the observation period. The simultaneous occurrence of aseismic-slip transients over a large area is consistent with large-scale slow unlocking processes preceding the Illapel mainshock.

Plain Language Summary The universality of precursory foreshock accelerations before large earthquakes is still controversial. We employ the template matching method to detect the small earthquakes and aseismic-slip transients before the 2015 Mw 8.4 Illapel earthquake. Our results show the large-scale aseismic-slip transients surrounding the impending Illapel rupture zone, suggesting a slow unlocking process. Our results have important implications on monitoring and time-dependent hazard assessment.

1. Introduction

Observations of precursory signals before large earthquakes are important in terms of earthquake forecasting and time-dependent hazard assessment. Foreshock sequences were observed to migrate toward and/or accelerate around the hypocenter of some recent large earthquakes. For example, intense foreshock sequences migrated toward the hypocenter starting from several days to weeks before the 2011 M 9.0 Tohoku-Oki earthquake and the 2014 M 8.2 Iquique earthquake (e.g., A. Kato et al., 2012; A. Kato & Nakagawa, 2014; Meng et al., 2015). Bouchon et al. (2013) found that a lot of large interplate earthquakes in the North Pacific were preceded by accelerating seismicity around the hypocenter starting from up to months prior to the mainshock. Aseismic slip has been suggested to be a driving force of these foreshock sequences based on statistical declustering analysis of earthquake catalogs, repeating earthquakes or Global Positioning System (GPS) observations. However, the universality of precursory foreshock accelerations before large earthquakes is still controversial, especially for those with no obvious foreshock sequences. On 16 September 2015, the Mw 8.4 Illapel earthquake ruptured on the west coast of central Chile where the Nazca plate is subducting underneath the South American Plate (Figure 1a). Based on the regional earthquake catalog, Papadopoulos and Minadakis (2016) identified slightly elevated seismic activities around the Illapel epicenter since ~3.5 months before the mainshock. But it is still not clear regarding the spatiotemporal scale and the driving mechanism of the preparatory process, which may involve seismic and aseismic slip processes on the plate boundary.

To investigate whether aseismic slip plays an important role in the preparatory process, a number of recent studies focused on detecting the aseismic-slip transients before large earthquakes. Aseismic slip can be directly captured by land-based GPS stations. But the GPS stations become less sensitive to deformation

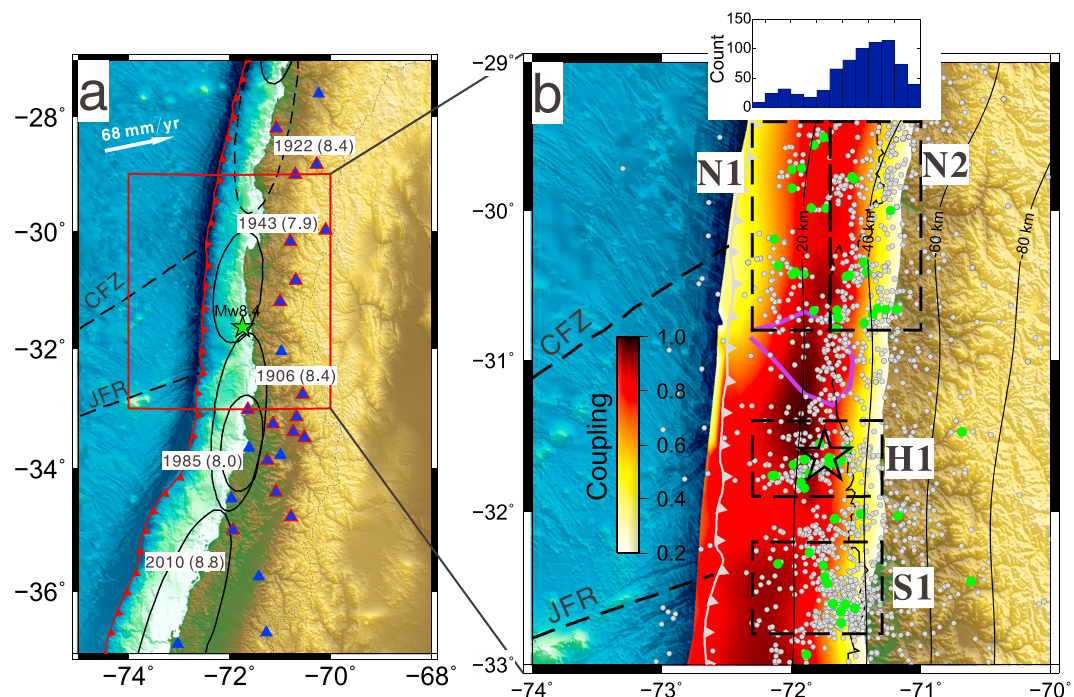


Figure 1. (a) Map showing the 27 stations used in the repeating earthquake analysis (blue triangles) and the subset of 17 stations used for matched-filter detection (blue triangles with red boundaries). The black and dashed ellipses denote maximal rupture zones of instrumental and historical megathrust earthquakes (Métois et al., 2012). The green star denotes the epicenter of the 2015 M 8.4 Illapel mainshock. The plate convergence rate (68 mm/year) is from Métois et al. (2012). The two dashed lines indicate the Challenger fracture zone (CFZ) and Juan-Fernandez Ridge (JFR). (b) The gray dots show the locations of premainshock events from the Centro Sismológico Nacional, Universidad de Chile. The green dots denote repeating earthquakes. N1, N2, H1, and S1 are four subregions for investigating the seismicity and aseismic-slip rates. The color scale denotes the model from Tilmann et al. (2016), which reflects plate coupling before the 2010 M 8.8 Maule earthquake. The purple curve denotes 5-m principal coseismic-slip contour of the 2015 M 8.4 Illapel earthquake from An and Meng (2016). The inset figure shows the histogram of the longitude of events within N1 and N2, which shows a bimodal distribution. The thin black contours show the Slab 1.0 geometry (Hayes et al., 2012).

transients in the offshore area. Alternatively, repeating earthquakes can be used to estimate the in situ aseismic slip on the plate boundary (e.g., Igarashi et al., 2003; Uchida & Matsuzawa, 2013). Repeating earthquakes (repeaters) refer to a series of seismic events with the same focal mechanisms at very close locations, producing almost identical waveforms. They are thought to represent recurrent ruptures of asperities driven to failure by surrounding aseismic slip (Nadeau & Johnson, 1998; Nadeau & McEvilly, 1999). Based on an empirical relation between seismic moment and aseismic slip (Nadeau & Johnson, 1998), repeaters can serve as a creep meter to directly measure the localized aseismic slip surrounding asperities on the plate boundary.

In this paper, we investigate the temporal evolutions of premainshock seismicity and aseismic slip around the 2015 Mw 8.4 Illapel rupture. To obtain a more complete earthquake catalog, we employ the matched filter method based on an enhanced template dataset to detect uncatalogued small events. Repeating earthquakes are then extracted to infer the amount of aseismic slip in each episode. Then we investigate the variations of seismicity and aseismic-slip rate in different regions around the mainshock rupture. Finally, we discuss our observations of wide aseismic-slip transients in terms of a large-scale slow unlocking process preceding the Illapel mainshock.

2. Data and Analysis

2.1. Matched-Filter Detection

We acquire three-component velocity seismograms recorded by 17 broadband seismic stations (Figure 1a) within 400 km from the Mw 8.4 epicenter (31.637°S , 71.741°W), determined by the Centro Sismológico

Nacional de Chile (CSN). The continuous seismograms span from 16 July 2011, the earliest time data was available, to 16 September 2015 (mainshock). Note that most of the stations started to record data since 28 April 2014 (Figure S1 in the supporting information), ~507 days before the mainshock. The template catalog is mostly from the CSN website (4195 events, [74°–70°W, 33°–29°S], from 16 July 2011 to 16 October 2015, <http://www.sismologia.cl>). To detect more potential earthquakes that repeat before the mainshock, we incorporate the newly detected repeating aftershocks of the Illapel earthquake (315 events, Huang et al., 2017) into the template data set.

We filter both the template and continuous seismograms with a passband from 1 to 6 Hz and downsample them to 20 Hz. We cut the 10-s long template waveforms starting from 5 s before the theoretical S arrival times, computed based on a local velocity model (Ruiz et al., 2016). To ensure enough data and high quality of template waveforms, we only retain the templates with at least nine channels and a signal-to-noise ratio larger than 5. The signal-to-noise ratio is estimated by comparisons of the template window with the noise window before the P arrival time. We compute cross-correlation coefficients (CC) between template and continuous waveforms, shifting the window with a step of one data point (0.05 s). Then the CC traces in each day are averaged over all channels after adjusting the traveltimes differences at different stations. We determine positive detections as having a threshold of 12 times the median absolute deviation of the CC traces in the day of interest (Text S1 and Figure S2, e.g., Peng & Zhao, 2009; A. Kato et al., 2016). To remove multiple detections associated with the same event, we assign the location of the template with the largest average CC to the detected event for the same segment of continuous records (over 5 s of overlap). Note that the locations of the detected events inherit the uncertainties from the CSN catalog, which is based on P, Pn, and S arrival times at the nearest stations (Ruiz et al., 2017). The mean location error of the CSN catalog is approximately 11 km (Figure S3) based on the comparison of the CSN catalog with two relocated aftershock catalogs (Herman et al., 2017; Ruiz et al., 2016). The origin time of the detected event is determined by adding the time difference of the template window and the detection window to the origin time of the template. The magnitude of the detected event is typically estimated by assuming that one-unit increase in magnitude corresponds to a tenfold increase in maximum absolute amplitude ratio (Peng & Zhao, 2009). To check if this assumption is valid for each station, we fit the relation between the maximum absolute amplitude ratio and magnitude difference for all template pairs within 30 km with the following function:

$$m_1 - m_2 = x_i \times \log_{10}(A_1/A_2),$$

where m_1 and m_2 are the local magnitudes (MI), A_1 and A_2 are maximum absolute amplitude within the S wave window, and x_i is the parameter to be determined at station i . We find that x_i is generally close to 1 with small variations among stations (Figure S4). We first estimate the magnitude of the detected event separately at each station according to the corresponding relation. Then the median value of all magnitudes is taken as the magnitude of the detected event.

2.2. Repeating Earthquakes

We extract repeating earthquakes ($Mw >= 2.5$) from the matched-filter-enhanced catalog (from July 2011 to mainshock) and CSN aftershocks (from mainshock to August 2016). The MI are converted to moment magnitudes (Mw) according to Meng et al. (2015):

$$Mw = (2/3)MI + 1.56 \text{ if } MI \leq 4.41$$

$$Mw = MI + 0.09 \text{ if } 4.41 < MI < 5.71$$

We perform cross correlations on vertical waveforms of all event pairs with hypocentral separations up to 30 km and depths smaller than 80 km. To include both P and S wave energy, we cut waveform windows starting from 10 s before the P arrival to 15 s after the S arrival. Compared to the matched-filter analysis, we focus on detecting relatively large repeaters ($Mw >= 2.5$). Therefore, we include all 27 stations within 600 km from the epicenter for analysis (Figure 1a). The different frequency bands are selected to approximately correspond to the source size (Igarashi et al., 2003; Meng et al., 2015): 1–4 Hz is applied for event pairs with both $Mw >= 3$ or 1–8 Hz for other pairs. We categorize event pairs as repeater pairs if the CC is larger than 0.95 and the magnitude difference (estimated from the amplitude ratio) is smaller than 0.5 at two or more stations (e.g., Figure S6). In addition, due to the fact that some stations are at close locations (Figure 1a), we require

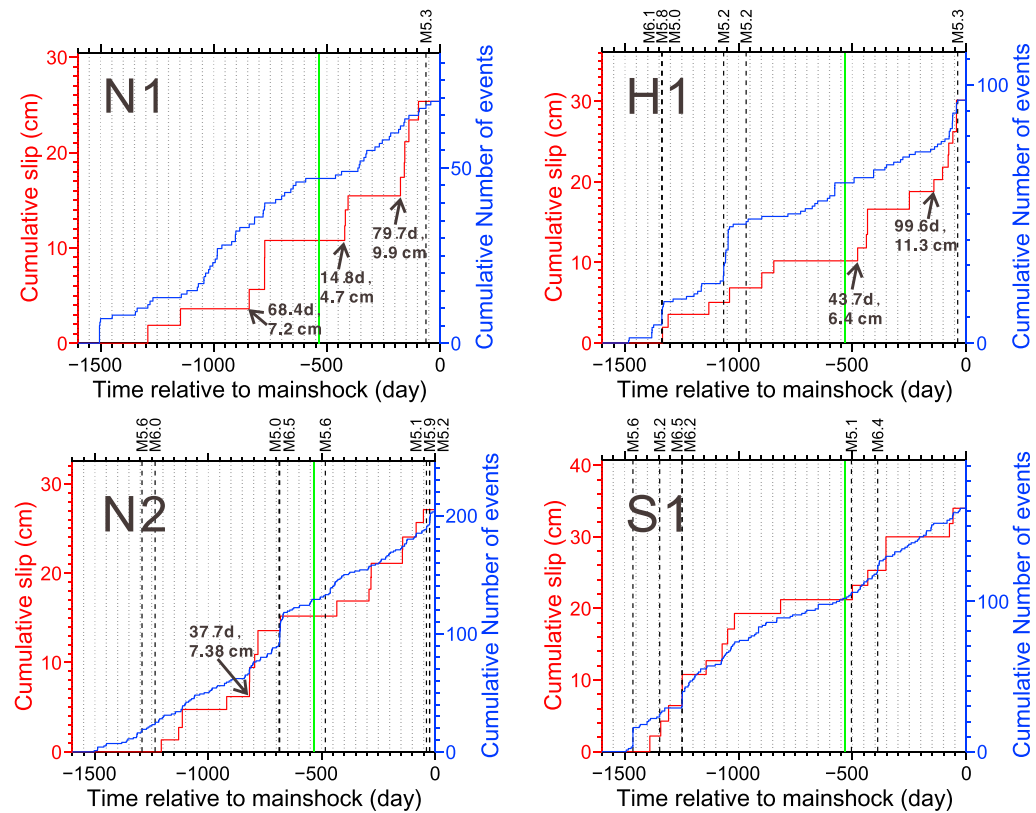


Figure 2. The cumulative number of seismicity (blue curves, $M > = 3.5$) and average cumulative aseismic slip (red curves) inferred from $M > = 3.0$ repeaters within the different regions shown in Figure 1b. Black vertical dashed lines denote $M > = 5.0$ events. The green line indicates the timing of the 1 April 2014 M 8.2 Iquique earthquake. The arrows mark the several short-duration aseismic-slip transients with durations and accumulated slip labeled aside.

that the station set used in identifying repeating earthquake pairs must span a distance larger than 50 km. Finally, different repeater pairs are linked into the same sequence if they share a common event.

3. Results

We detect a total of 9,273 new events within [74°W–70°W, 33°S–29°S] before the Mw 8.4 Illapel mainshock, ~3.3 times more than the CSN catalog (2,795 events), under the threshold of 12 times the median absolute deviation. We apply the best combined method (Wiemer, 2001) to estimate the magnitude of completeness (Mc). The Mc of the enhanced catalog is ~2.8 while that of the CSN catalog is ~3.4 (Text S1 and Figure S7). As the number of stations changes significantly from 28 April 2014 (Figure S1), the capability of detecting small events may vary correspondingly. We estimate the temporal variation of Mc with a moving window of 500 events with 50% overlap (Wiemer, 2001). The Mc is within ~2.5–3.0 before April 2014 but decreases to ~2–2.5 afterward (Figure S8). Taking account of uncertainties of the estimated Mc, we set the magnitude cutoff to be M 3.5 for seismicity to ensure a consistent level of completeness in the study period.

Among the enhanced catalog, 791 repeating earthquakes (302 sequences) within the magnitude range of Mw 2.72 to 5.19 are identified, including 181 repeaters before and 610 repeaters after the mainshock. Most of the repeater sequences (206 out of 302) are doublets (only two events in one sequence). To estimate the aseismic-slip increments surrounding a repeater sequence, we convert the seismic moment of composite repeaters to aseismic slip according to the empirical relation by Nadeau and Johnson (1998). We retain repeater sequences with the mean magnitude larger than M 3.0 to calculate the cumulative slip. Note that the detection of repeaters between M 3.0 and 3.5 may be incomplete at some short time periods before 2014 due to the fluctuations of Mc (Figure S8). This procedure may underestimate the total accumulated slip and uncertainties exist for using the Nadeau and Johnson's (1998) relation; therefore, here we focus on

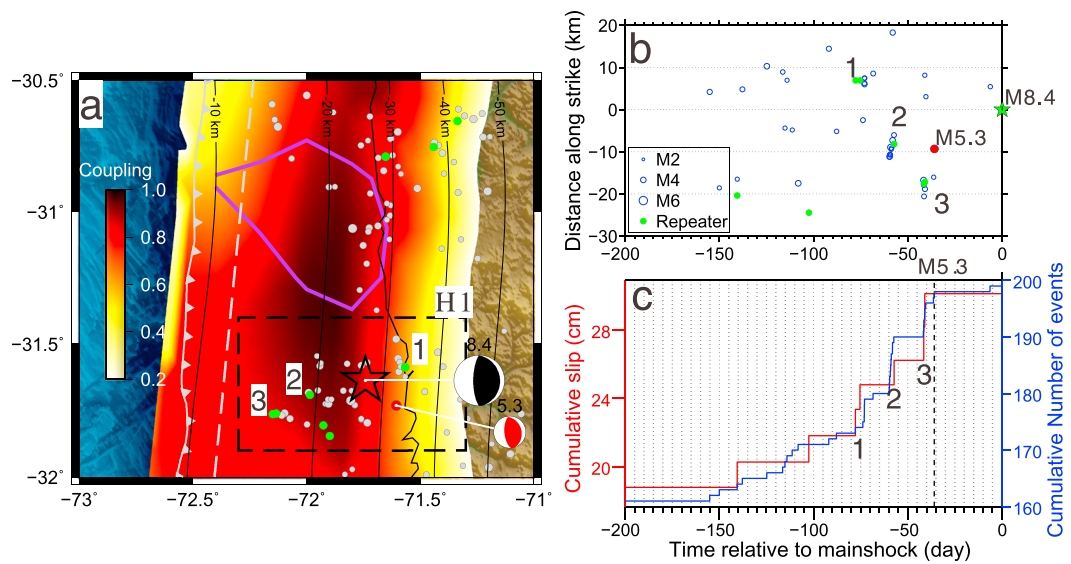


Figure 3. (a) A zoom-in map of region H1 (dashed rectangle, Figure 1b) with $M >= 3.0$ seismicity (gray dots) and repeaters (green dots) within the last 200 days before the mainshock. The focal mechanisms of the M 5.3 event and the mainshock are from U.S. Geological Survey National Earthquake Information Center. (b) The along-strike distance of seismicity within region H1 projected onto the gray dashed line in (a). (c) The cumulative number of events (blue) and aseismic slip (red). Note the quiescence of seismicity and repeaters after the M 5.3 event, lasting for ~36 days until the mainshock.

comparing the temporal change of the aseismic-slip rate. We estimate the cumulative aseismic slip within different regions around the mainshock rupture by averaging the cumulative aseismic-slip series from individual repeater sequences (e.g., Uchida et al., 2016). Four regions are selected based on the distribution of repeaters and seismicity (Figure 1b): N1 and N2 (updip and downdip areas to the north of rupture zone), H1 (around the epicenter), and S1 (away from rupture zone). Regions N1 and N2 are divided according to the bimodal distribution of seismicity in the along-dip direction (Figure 1b).

Within region N1, the aseismic-slip episodes correspond to the periods with elevated seismicity rate. From ~ -175 to -95 days, the aseismic slip accumulates the largest amount (~ 9.9 cm) within the observation period (Figure 2). There are also two other aseismic-slip transients around -850 and -420 days with shorter duration and less amount of slip. In contrast, within the downdip region N2, the aseismic-slip rate is relatively stable with short-duration episodes concurrent with increasing seismicity rate. For example, the aseismic-slip episode around -818 days is accompanied with elevated seismicity rate and leads to a M 5.0 event immediately followed by a M 6.5 event (Figure 2).

Within region H1, the aseismic-slip rate is relatively stable before -500 days. The simultaneous acceleration in seismicity and aseismic slip start from ~ 140 days before the mainshock. This episode accumulates the largest amount of slip (~ 11.3 cm). This acceleration culminates in a M 5.3 event at ~ -36 days, followed by a relative quiescence in both seismicity and repeaters until the mainshock (Figures 3a–3c). Another aseismic-slip transient occurred at ~ -476 days with shorter duration (43.7 days) and less amount of slip (6.4 cm). Within region S1, from $-1,500$ to $-1,000$ days, the rates of seismicity and aseismic slip appear to increase after several $M >= 5$ events then slowly decay with time. This may indicate triggered aftershock sequences and afterslip. It is notable that the seismicity appears to accelerate after the 2014 Mw 8.2 Iquique earthquake which is $\sim 1,431$ km away. This might reflect the dynamic triggering effect of the Iquique event, which is expected to induce a dynamic stress change of ~ 72 kPa according to Van der Elst and Brodsky (2010). We perform several tests to verify that the general patterns of temporal variations of aseismic-slip rates, especially the last most significant aseismic-slip episode in N1 and H1, are consistent under more strict detection criteria of repeaters (Text S2 and Figures S9–S13).

We estimate the aseismic moment within different regions by assuming grids with different sizes (0.05° , 0.1° , and 0.15° , Figures 4a and S14) surrounding the repeaters (Meng et al., 2015). This is based on the assumption

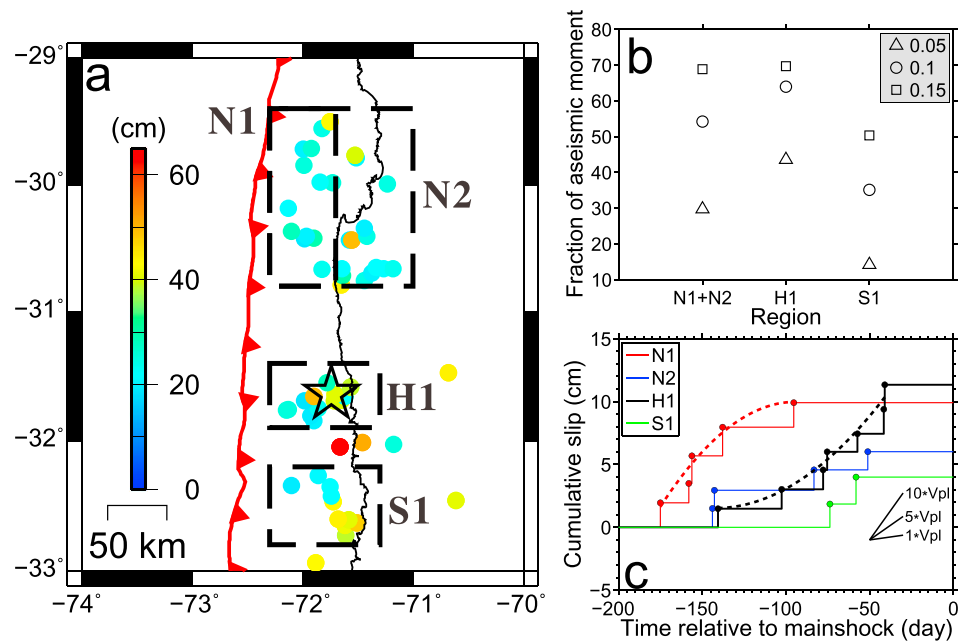


Figure 4. (a) The dots show the locations of repeating earthquake sequences before the 2015 Mw 8.4 Illapel event (black star), colored by the cumulative aseismic slip during the ~4-year period before the mainshock. (b) The proportion of aseismic moment among the total moment (seismic + aseismic) under the assumption of different sizes of grids around repeaters (0.05°, 0.1°, and 0.15°, Figure S14). (c) The comparison of aseismic-slip series within the last 200 days. The dashed lines are the quadratic fits of the cumulative aseismic slip for region N1 and H1. The plate convergence rate (V_{pl}) is 68 mm/year (Métois et al., 2012).

that the aseismic slip is colocated with the repeaters, which is validated by our recent study of afterslip and aftershocks wrapping around the Illapel rupture (Huang et al., 2017). A grid size with 0.15° leads to estimations of aseismic afterslip moment closest to the geodetic measurements for the Illapel earthquake (Huang et al., 2017). Assuming a crustal shear modulus of 30 GPa and patch sizes of 0.05°, 0.1°, and 0.15°, the repeater-inferred aseismic moment release in different regions is similar: Mw 6.18–6.70, Mw 6.20–6.69, Mw 6.20–6.51, and Mw 6.21–6.74 in regions N1, N2, H1, and S1, respectively. The seismic moment within each region is Mw 5.62, Mw 6.63, Mw 6.27, and Mw 6.73 for N1, N2, H1, and S1, respectively, obtained by summing all $M > = 3.0$ events. We estimate the fraction of aseismic moment among the total moment (seismic + aseismic) within regions N1 + N2 (combining N1 and N2), H1, and S1 to be ~69%, 70%, and 50% for the grid size of 0.15°, respectively (Figure 4b). Regions N1 and N2 are combined to be in better comparison with other regions in the along-strike direction. Note that the fraction of aseismic moment within region N1 is larger than 95%, implying that the moment release is almost purely aseismic at the region close to the trench (Figure S15). In addition, we also fit the aseismic-slip series within the last 200 days with a quadratic function (Figure 4c), which fits better than the linear function (Figure S16). It suggests that the aseismic slip exhibits progressive accelerations within H1 while it decelerates in N1.

4. Discussion and Conclusion

By applying the matched-filter method based on an enhanced template data set including the repeating aftershocks, we detect 9,273 new events (including 181 repeating earthquakes) in an ~4-year period before the 2015 Mw 8.4 Illapel earthquake. Within the last ~170 days, aseismic-slip transients inferred from repeating earthquakes are most significant at both sides of the principal Illapel rupture zone. We interpret them as the large-scale slow unlocking process preceding the 2015 Mw 8.4 Illapel earthquake in the late interseismic period. Moreover, the last episode of seismicity and aseismic slip around the epicenter exhibit simultaneous progressive accelerations, suggesting the interplay of seismic and aseismic slip.

Laboratory studies found a nucleation phase manifested by accelerations in foreshocks immediately before the mainshock (e.g., Ohnaka & Shen, 1999). Observations of recent large earthquakes suggest that the nucleation phase can be extended both in time (days to years) and space (hundreds of kilometers; e.g., Bouchon et al., 2011, 2013; A. Kato et al., 2012; Socquet et al., 2017). For example, before the 2011 M 9.0 Tohoku-Oki earthquake, two foreshock sequences migrated toward the epicenter from ~40 km away, starting from ~30 and 2 days before the mainshock, respectively. Further studies showed that there are decadal accelerations in aseismic slip with a lateral dimension of ~300 km before the Tohoku-Oki earthquake (Mavrommatis et al., 2015). In comparison, before the 2014 Mw 8.2 Iquique earthquake, a 2-week long foreshock sequence migrated from ~40 km away toward the epicenter (Meng et al., 2015). Other studies revealed an 8-month slow slip before the Iquique earthquake by background seismicity rate and repeating earthquakes (A. Kato et al., 2016) and GPS observations (Socquet et al., 2017). For the case of the 2015 Illapel earthquake, the large-scale aseismic-slip transients occur within the last ~170 days and surround the mainshock slip patch. This can be explained by the large-scale unlocking process involving aseismic slip, consistent with the frequent aseismic-slip episodes observed in the late stage of numerical cycle simulations of megathrust earthquakes (e.g., Ohtani et al., 2014). Due to the limitations of continuously operating seismic network for repeater analysis, it is not clear whether a decade-long accelerated unlocking (Mavrommatis et al., 2015) or periodic slow slip (years) as seen in the NE Japan subduction zone (Uchida et al., 2016) occurs prior to the Illapel earthquake.

Repeating earthquakes are mostly located at two sides of the Illapel coseismic slip zone. By investigating the swath bathymetric data, Poli et al. (2017) found that the bending slab fractures seaward to the trench show a rotation from a NE-SW direction south of ~31°S to an almost N-S strike in the north. They also found correlations between the distribution of repeating aftershocks and the fracture networks (Figure 3 of Poli et al., 2017). The preseismic repeaters identified in our study are consistent with these observations. The high pore fluid pressure around the fractures may be responsible for the swarms and repeaters (Poli et al., 2017). These repeaters may be surrounded by velocity strengthening regions as illuminated by large afterslip (Huang et al., 2017). Around the Illapel slip patch, stresses are easy to build up due to the episodic loading of aseismic-slip transients. In addition, the relatively concentrated repeaters around the Illapel hypocenter may lead to more concentrated stresses loaded by aseismic slip compared to the region to the north, where the repeaters are more widely distributed. Therefore, the hypocentral area may be easier than the north to reach the critical stress required for the rupture initiation.

In the hypocentral area H1, three clusters including repeaters (1–3, Figure 3) occurred within the last 150 days. Clusters 2 and 3 occurred later but were located updip from cluster 1. The possible mechanisms for connecting these clusters are the slow slip, fluid flow, pressure transients, or stress transfer. The largest events in clusters 1–3 are M 3.8, M 4.6, and M 4.2, respectively. Assuming a stress drop of 3 MPa, the source radius is ~633, 1258, and 860 m, significantly smaller than the distances (~41.4 and 14.4 km) between them. Note that the distance between clusters 2 and 3 (14.4 km) is close to the possible location error (see section 2.1 and Figure S3). The triggering potential of static stress changes is generally confined within one or two source dimensions (Hill & Prejean, 2015). Therefore, the stress transfer is unlikely the triggering mechanism connecting these clusters. Another possibility is the slow slip transients, supported by the observed repeaters among the clusters. We consider the fluid flow or pressure transients less likely as significant afterslip occurs at the similar location and the repeaters persist in a long time period after the mainshock (Huang et al., 2017). It is notable that the M 5.3 event occurred after cluster 3 that is located ~50 km updip. This may indicate that there was ongoing aseismic slip or smaller earthquakes around the M 5.3 event which eventually trigger it.

It is interesting to observe that the acceleration in seismicity and aseismic slip around the hypocenter leads up to a M 5.3 event, followed by ~36 days of quiescence in both seismicity and repeaters. The M 5.3 event is located close to the Illapel epicenter (~16.6 km to the southeast) with a low-angle thrust mechanism similar to the Illapel mainshock (Figure 3a). This quiescence is anomalous in the sense that the M 5.3 event was not followed by a typical aftershock sequence following Omori's law, which implies that the aftershock productivity is very low. The comparison with other aftershock sequences in the study region shows that the M 5.3 event has fewer number of aftershocks than most of the M 5.0–5.6 events (Figure S17). One possible explanation is that the aseismic-slip transients before the M 5.3 event occur in a relatively large scale so that they depleted completely the accumulated stresses on the small asperities (including repeaters) around the M 5.3 event. After the loading of the aseismic-slip transients and the M 5.3 event, the Illapel mainshock patch

is brought closer to failure. The 36-day long quiescence period between the M 5.3 event and the mainshock is intriguing. The quiescence is also observed in earthquake cycle simulations where it sometimes lasts for several years (e.g., N. Kato et al., 1997). Luo and Ampuero (2018) performed numerical simulations on a fault model with spatially variable frictional properties and pore pressure. They found that the increasing pore pressure could change the relative strength between velocity weakening and velocity strengthening asperities. As a result, a period of stable slip (quiescence) occurs prior to the dynamic rupture. This might be the case before the Illapel earthquake as the pore pressure can be elevated if fluids are released through the fracture zones. The short-term anomalous quiescence period is also seen during 1 week before the 2014 Mw 8.2 Iquique earthquake (Meng et al., 2015) and ~8 days before the largest Mw 7.3 foreshock of the Tohoku-Oki earthquake (A. Kato et al., 2012). It is thus important to better understand the mechanism of the different durations of quiescence before large earthquakes. A systematic investigation of the relation of spatiotemporal scale of quiescence with the fault properties, stress state of the fault, and the dimension of impending large earthquakes may shed some new insights on mainshock nucleation processes.

Our results suggest that the aseismic-slip transients within the last episode are more significant at areas around the Illapel rupture zone than areas further away from the rupture. The fraction of aseismic moment also appears to be the largest in the hypocentral area (Figure 4b). Moreover, the aseismic-slip rate is gradually increasing with time around the hypocentral area (Figure 4c). Therefore, temporal variations of repeater-inferred aseismic-slip rates may serve as an additional important tool in monitoring and time-dependent hazard assessment. The aseismic-slip transients as seen in this study are located offshore and last less than 100 days. They are likely close to or below the detection threshold by GPS observations. Our preliminary analysis shows that the general trend presented at some GPS stations is consistent with the expected displacement based on repeater data, although the amplitude of the signal is on the same order as the background noise in the GPS data (Text S3 and Figures S18–S20). A recent study by Gardonio et al. (2017) also showed that small repeating earthquakes ($M > = 1$) can be used to detect slow-slip episodes missed by GPS observations. Although several large earthquakes including the 2010 M 8.8 Maule, the 2014 M 8.2 Iquique, and the 2015 M 8.4 Illapel earthquake have ruptured different parts of the Chilean margin, there are still large areas with high seismic coupling and significant moment deficit (e.g., Schurr et al., 2014). Integrated observations of seismicity, repeating earthquakes, and geodetic observations at the transition from low to high coupling areas are important and can potentially improve time-dependent earthquake forecasting models.

Acknowledgments

We thank Editor Gavin Hayes and two anonymous reviewers for constructive comments that greatly improved the manuscript. We also thank Zhengkang Shen for his guidance on analyzing GPS data. The IRIS (www.iris.edu) data manager centers provided access to broadband seismograms used in this study. This work relies on the computational and storage services associated with the Hoffman2 Shared Cluster provided by UCLA Institute for Digital Research and Education's Research Technology Group. This study is supported by the Leon and Joann V. C. Knopoff foundation, by National Science Foundation EAR-1723192, and by the 2017 UCLA Big Data Initiative.

References

- An, C., & Meng, L. (2016). Application of array backprojection to tsunami prediction and early warning. *Geophysical Research Letters*, 43, 3677–3685. <https://doi.org/10.1002/2016GL068786>
- Bouchon, M., Durand, V., Marsan, D., Karabulut, H., & Schmittbuhl, J. (2013). The long precursory phase of most large interplate earthquakes. *Nature Geoscience*, 6(4), 299–302. <https://doi.org/10.1038/ngeo1770>
- Bouchon, M., Karabulut, H., Aktar, M., Özalbayev, S., Schmittbuhl, J., & Bouin, M. P. (2011). Extended nucleation of the 1999 Mw 7.6 Izmit earthquake. *Science*, 331(6019), 877–880. <https://doi.org/10.1126/science.1197341>
- Gardonio, B., Marsan, D., Socquet, A., Bouchon, M., Jara, J., Sun, Q., et al. (2017). Revisiting slow slip events occurrence in Boso Peninsula, Japan, combining GPS data and repeating earthquakes analysis. *Journal of Geophysical Research: Solid Earth*, 123, 1502–1515. <https://doi.org/10.1002/2017JB014469>
- Hayes, G. P., Wald, D. J., & Johnson, R. L. (2012). Slab1. 0: A three-dimensional model of global subduction zone geometries. *Journal of Geophysical Research*, 117, B01302. <https://doi.org/10.1029/2011JB008524>
- Herman, M. W., Nealy, J. L., Yeck, W. L., Barnhart, W. D., Hayes, G. P., Furlong, K. P., & Benz, H. M. (2017). Integrated geophysical characteristics of the 2015 Illapel, Chile, earthquake. *Journal of Geophysical Research: Solid Earth*, 122, 4691–4711. <https://doi.org/10.1002/2016JB013617>
- Hill, D. P., & Prejean, S. G. (2015). Dynamic triggering. In H. Kanamori (Ed.), *Treatise on geophysics* (2nd ed., Vol. 4, chap. 8, pp. 273–304). Oxford, UK: Elsevier.
- Huang, H., Xu, W., Meng, L., Bürgmann, R., & Baez, J. C. (2017). Early aftershocks and afterslip surrounding the 2015 Mw 8.4 Illapel rupture. *Earth and Planetary Science Letters*, 457, 282–291. <https://doi.org/10.1016/j.epsl.2016.09.055>
- Igarashi, T., Matsuzawa, T., & Hasegawa, A. (2003). Repeating earthquakes and interplate aseismic slip in the northeastern Japan subduction zone. *Journal of Geophysical Research*, 108(B5), 2249. <https://doi.org/10.1029/2002JB001920>
- Kato, A., Fukuda, J. I., Kumazawa, T., & Nakagawa, S. (2016). Accelerated nucleation of the 2014 Iquique, Chile Mw 8.2 earthquake. *Scientific Reports*, 6(1), 24792. <https://doi.org/10.1038/srep24792>
- Kato, A., & Nakagawa, S. (2014). Multiple slow-slip events during a foreshock sequence of the 2014 Iquique, Chile Mw 8.1 earthquake. *Geophysical Research Letters*, 41, 5420–5427. <https://doi.org/10.1002/2014GL061138>
- Kato, A., Obara, K., Igarashi, T., Tsuruoka, H., Nakagawa, S., & Hirata, N. (2012). Propagation of slow slip leading up to the 2011 Mw 9.0 Tohoku-Oki earthquake. *Science*, 335(6069), 705–708. <https://doi.org/10.1126/science.1215141>
- Kato, N., Ohtake, M., & Hirasawa, T. (1997). Possible mechanism of precursory seismic quiescence: Regional stress relaxation due to preseismic sliding. *Pure and Applied Geophysics*, 150(2), 249–267. <https://doi.org/10.1007/s000240050075>

- Luo, Y., & Ampuero, J. P. (2018). Stability of faults with heterogeneous friction properties and effective normal stress. *Tectonophysics*, 733, 257–272.
- Mavromatis, A. P., Segall, P., Uchida, N., & Johnson, K. M. (2015). Long-term acceleration of aseismic slip preceding the Mw 9 Tohoku-oki earthquake: Constraints from repeating earthquakes. *Geophysical Research Letters*, 42(22), 9717–9725. <https://doi.org/10.1002/2015GL066069>
- Meng, L., Huang, H., Bürgmann, R., Ampuero, J. P., & Strader, A. (2015). Dual megathrust slip behaviors of the 2014 Iquique earthquake sequence. *Earth and Planetary Science Letters*, 411, 177–187. <https://doi.org/10.1016/j.epsl.2014.11.041>
- Métois, M., Socquet, A., & Vigny, C. (2012). Interseismic coupling, segmentation and mechanical behavior of the central Chile subduction zone. *Journal of Geophysical Research*, 117, B03406. <https://doi.org/10.1029/2011JB008736>
- Nadeau, R. M., & Johnson, L. R. (1998). Seismological studies at Parkfield VI: Moment release rates and estimates of source parameters for small repeating earthquakes. *Bulletin of the Seismological Society of America*, 88(3), 790–814.
- Nadeau, R. M., & McEvilly, T. V. (1999). Fault slip rates at depth from recurrence intervals of repeating microearthquakes. *Science*, 285(5428), 718–721. <https://doi.org/10.1126/science.285.5428.718>
- Ohnaka, M., & Shen, L. F. (1999). Scaling of the shear rupture process from nucleation to dynamic propagation: Implications of geometric irregularity of the rupturing surfaces. *Journal of Geophysical Research*, 104(B1), 817–844. <https://doi.org/10.1029/1998JB900007>
- Ohtani, M., Hirahara, K., Hori, T., & Hyodo, M. (2014). Observed change in plate coupling close to the rupture initiation area before the occurrence of the 2011 Tohoku earthquake: Implications from an earthquake cycle model. *Geophysical Research Letters*, 41(6), 1899–1906. <https://doi.org/10.1002/2013GL058751>
- Papadopoulos, G. A., & Minadakis, G. (2016). Foreshock patterns preceding great earthquakes in the subduction zone of Chile. *Pure and Applied Geophysics*, 173(10–11), 3247–3271. <https://doi.org/10.1007/s00424-016-1337-5>
- Peng, Z., & Zhao, P. (2009). Migration of early aftershocks following the 2004 Parkfield earthquake. *Nature Geoscience*, 2(12), 877–881. <https://doi.org/10.1038/ngeo697>
- Poli, P., Jeria, A. M., & Ruiz, S. (2017). The Mw 8.3 Illapel earthquake (Chile): Preseismic and postseismic activity associated with hydrated slab structures. *Geology*, 45(3), 247–250. <https://doi.org/10.1130/G38522.1>
- Ruiz, S., Klein, E., del Campo, F., Rivera, E., Poli, P., Métois, M., et al. (2016). The seismic sequence of the 16 September 2015 Mw 8.3 Illapel, Chile, earthquake. *Seismological Research Letters*, 87(4), 789–799. <https://doi.org/10.1785/0220150281>
- Ruiz, S., Moreno, M., Melnick, D., Campo, F., Poli, P., Baez, J. C., et al. (2017). Reawakening of large earthquakes in South-Central Chile: The 2016 Mw7.6 Chiloé event. *Geophysical Research Letters*, 44, 6633–6640. <https://doi.org/10.1002/2017GL074133>
- Schurr, B., Asch, G., Hainzl, S., Bedford, J., Hoechner, A., Palo, M., et al. (2014). Gradual unlocking of plate boundary controlled initiation of the 2014 Iquique earthquake. *Nature*, 512(7514), 299–302. <https://doi.org/10.1038/nature13681>
- Socquet, A., Valdes, J. P., Jara, J., Cotton, F., Walpersdorf, A., Cotte, N., et al. (2017). An 8 month slow slip event triggers progressive nucleation of the 2014 Chile megathrust. *Geophysical Research Letters*, 44(9), 4046–4053. <https://doi.org/10.1002/2017GL073023>
- Tilmann, F., Zhang, Y., Moreno, M., Saul, J., Eckelmann, F., Palo, M., et al. (2016). The 2015 Illapel earthquake, Central Chile: A type case for a characteristic earthquake? *Geophysical Research Letters*, 43(2), 574–583. <https://doi.org/10.1002/2015GL066963>
- Uchida, N., Iinuma, T., Nadeau, R. M., Bürgmann, R., & Hino, R. (2016). Periodic slow slip triggers megathrust zone earthquakes in northeastern Japan. *Science*, 351(6272), 488–492. <https://doi.org/10.1126/science.aad3108>
- Uchida, N., & Matsuzawa, T. (2013). Pre-and postseismic slow slip surrounding the 2011 Tohoku-oki earthquake rupture. *Earth and Planetary Science Letters*, 374, 81–91. <https://doi.org/10.1016/j.epsl.2013.05.021>
- Van Der Elst, N. J., & Brodsky, E. E. (2010). Connecting near-field and far-field earthquake triggering to dynamic strain. *Journal of Geophysical Research*, 115, B07311. <https://doi.org/10.1029/2009JB006681>
- Wiemer, S. (2001). A software package to analyze seismicity: ZMAP. *Seismological Research Letters*, 72(3), 373–382. <https://doi.org/10.1785/gssrl.72.3.373>